RTK-LoRa: High-Precision, Long-Range and Energy-Efficient Localization for Mobile IoT devices

Article *in* IEEE Transactions on Instrumentation and Measurement · December 2020

DOI: 10.1109/TIM.2020.3042296

4 authors, including:

Philipp Mayer
ETH Zurich
47 PUBLICATIONS **535** CITATIONS
SEE PROFILE

Michele Magno
ETH Zurich
332 PUBLICATIONS **5,951** CITATIONS
SEE PROFILE

This article has been accepted for publication in the IEEE Transactions on Instrumentation and Measurement.
Content may change prior to final publication. DOI: 10.1109/TIM.2020.3042296

RTK-LoRa: High-Precision, Long-Range and Energy-Efficient Localization for Mobile IoT devices

Philipp Mayer*, Michele Magno*, Armin Berger*, and Luca Benini*°
*Dept. of Information Technology and Electrical Engineering, ETH Zurich, Switzerland
°Dept. of Electrical, Electronic and Information Engineering, Università di Bologna, Italy

***Abstract* – High precision Global Navigation Satellite System (GNSS) is a crucial geo-localization feature enabling a wide range of applications, from mobile Internet of Things devices to autonomous drones and self-driving vehicles. Real-Time Kinematic (RTK) is a GNSS technology that attracting increased interest due to the centimeter precision achievable when wireless communication is present on the devices. On the other hand, sending continuously wireless data increases the energy consumption and the cost of the solution, especially when communication is carried over the 4G network. Due to those drawbacks, RTK is not much exploited in the localization of battery-operated devices. This work combines RTK with low-power long-range communication to achieve sub-meter precision in an energy-efficient RTK-based system. The proposed system exploits a state-of-the-art RTK-GNSS module combined with a long-range and low-power radio (LoRa) to achieve geo-localization with minimal wireless radio infrastructure requirements. An energy-efficient algorithm is proposed and implemented in a microcontroller to have a quick start-up and high accuracy. We evaluate three different GNSS modules and compare their performance in terms of power and accuracy. Experimental results, with in-field measurements, show that an average geo-localization precision of tens of centimeters is achievable on a battery-operated wireless end-node connected to a single base station used as a geostationary reference anchor placed at kilometers of distance. The peak precision measured is below 10 cm.**

Keywords — Low Power Sensors, Geo-Localization, Energy Efficiency, RTK, LoRa.

I. INTRODUCTION

The Global Navigation Satellite System (GNSS) is a crucial technology in navigation devices. Today, position information is widely available, as almost every smartphone, car, and smart mobile device has a GNSS module on-board. GNSS positioning works by measuring distances to satellites, so-called pseudo ranges. The positions/trajectories of the satellites are known and with the triangulation algorithm, it is possible to have the absolute position of the device. In GNSS, a minimum of 4 pseudo-ranges to 4 different satellites are required [1]. The pseudo-range is obtained from the time difference of the satellite signal transmission and reception time. Although GNSS is popular, its accuracy is low, with ranges of 2-3 m. This accuracy is enough for navigation. However, it is insufficient for more demanding applications, such as in self-driving vehicles, where cm accuracy is necessary for collision avoidance [2].

A recent method to improve the GNSS's accuracy and precision is the usage of differential GNSS (DGNSS) [2]. Real-Time Kinematic (RTK) GNSS is based on a base station module with a fixed precisely-known position and a mobile end-device called rover. In RTK, the base station sends information that allows the rover to improve its positioning accuracy when it has at least five satellites in common with the base station [3]. DGNSS with RTK techniques improves the accuracy up to the centimeter range [3].

Usually, GNSS systems for vehicles and mobile devices are coupled with a 3G/4G wireless interface that allows sending the position information to a remote host to track the mobile device. However, for low-power, battery-operated devices, 3G/4G is inconvenient to exchange the needed data for RTK DGNSS. This is mainly due to the power consumption and the fact the interface requires a network operator, and therefore it is not possible to have a direct connection between rover and base station in an inexpensive way.

In this work, we focus on long-range low-power wireless communication in the ISM narrow band (usually 868 MHz) to enable RTK and achieve high accuracy and energy efficiency. In this context, Long Range (LoRa) appears to be particularly promising, especially for the mW range power consumption, which is making it popular for many IoT applications [4], [5], [6]. A LoRa link allows transmission over kilometer range without the use of third-party network operators.

Another down-side of both DGNSS and GNSS is the high power consumption, which can be a critical issue for battery-operated mobile devices that need to work for long periods. Although localization systems can be supplied in some cases by the vehicle battery, in many applications (e.g., logistic containers [7]), it is impossible to access the mains power or the asset's battery/power. The requirement to stay operational without draining the auxiliary batteries is particularly relevant if vehicles are parked over more extended periods. As a result, individual battery-operated GNSS sensors cannot be located, and they get lost together with the tracked asset [2], [3]. Providing position information while achieving a long lifetime is a critical target for many application scenarios [6], [8], [9]. To achieve energy efficiency and to reduce the overall power consumption, most of today's battery-operated devices are periodically activated and turn-off power-hungry subsystems when not needed. However, there is even a further issue for GNSS due to the long period to acquire the satellite position after a cold start [10]. Due to these multiple, intertwined challenges, designing an energy-efficient high-precision GNSS system requires hardware and software co-design [11].

This paper extends the work in [12], where preliminary architecture and results have been presented. In this paper, an optimized architecture of the end-node, which achieves highly accurate localization and allows to trade-off between accuracy and energy consumption, is presented in detail. The proposed energy-efficient algorithm and its implementation

TABLE I COMPARISON RTK ENABLED GNSS SYSTEMS WITH LORA COMMUNICATION

	Commercial Receiver				Research	
	Reach RS2	FieldBee L2	RTK-M100R	UNI-GR1	IPSN'18	**This Work**
Company	EMLID	eFarmer B.V	Locosys	marxact	-	-
GPS Bands	L1, L2	L1, L2	L1, L2, L5	L1, L2, L5	L1, L2	L1, L2, L5
Channels	184	184	64	432	72	184
Update rate	up to 10 Hz	1-20 Hz	1-5 Hz	up to 20 Hz	up to 8 Hz	up to 20 Hz
Peak Precision RTK (H)	7 mm, +1 ppm CEP	10 mm, +1 ppm CEP	10 mm, +1 ppm CEP	10 mm, +1 ppm CEP	25 mm, +1 ppm CEP	10 mm, +1 ppm CEP
First RTK Fix	5 s	< 60 s	-	< 45 s	< 60 s	13 s
Power	< 2.5 W	4 W	< 2.5 W	< 3.7 W	300 mW active 100 uW idle	320 mW active 19 uW idle
Wireless Interface	3.5G, WiFi, Bluetooth, LoRa	WiFi, Bluetooth, optional LoRa	4G, LoRa	4G, WiFi, Bluetooth, LoRa, NFC	LoRa (SX1276)	LoRa (SX1261)

is illustrated and evaluated with in-field measurements. The main contributions of this paper and the improvements with respect to [12] can be summarized as follows:

1) An improved GNSS-RTK implementation with the capability of Assisted GNSS, reducing the time to first RTK fix by up to 20 s, and the energy consumption in duty cycled operation by 53 %.
2) The characterization of state-of-the-art GNSS and GNSS-RTK modules from different initial conditions and the influence on the time-to-first-fix.
3) A comparison of the implementations as a trade-off between localization accuracy and energy consumption, including an experimental evaluation to demonstrate the benefits of our solution.
4) In-field measurements, performed in the urban area of Zurich, Switzerland, demonstrating the operation in a real-world scenario.

II. Related Works

There is significant growth in research for improving the accuracy and reliability of outdoor localization systems based on GNSS for a wide range of application scenarios [13]–[21]. An extensive literature review is presented in [13] where a multitude of solutions and applications aiming to increase integrity and accuracy are presented. Another survey presented in [14] illustrates the features of commercial GNSS modules hosted by smartphones. The authors in [15] analyze the multipath effect, especially in an urban area, and show a solution to mitigate the influence, achieving an accuracy of a few meters. Accuracy is always one of the most pursued goals in research, and many solutions are proposing the combination of GNSS with other technologies to increase reliability and integrity. The authors in [16] present a reliable solution where they combine microelectromechanical systems (MEMS) sensors and a dual-antenna receiver. Their main goal is to increase the robustness of GNSS with industrial-grade inertial measurement units (IMUs) to get both better precision and quality of service at weak satellite connections.

Another key investigated research topic in GNSS is the widening of application scenarios enabled by reducing energy consumption. For instance in [17], the authors present the energy performance of commercial GNSS modules and propose energy-aware software scheduling algorithms to allow accurate trajectory tracking with increased energy efficiency. With the same goal in mind, the authors in [18] propose a solution where the GNSS data processing is offloaded in the cloud. However, this solution pays the improvement of energy efficiency with a low quality of service and high latency, plus the requirement of an Internet connection. A solution based on NB-IoT and GNSS confirms the direction of using GNSS combined with the Internet or the cloud to exploit the availability of data from the cloud. In contrast with the previous work, we combine the GNSS featured Real-Time Kinematic with LoRa to improve the accuracy and latency, improving as well the energy efficiency.

The capability of RTK-GNSS to improve the positioning accuracy is demonstrated in many recent works where novel RTK-GNSS features are evaluated and exploited in various application scenarios. The authors in [19] have performed an extensive evaluation of commercial low-cost RTK modules. Previous works show that both academic and industrial solutions allow reaching an accuracy of a few cm. In [20], the authors use the high precision for multi-drone operation. The solution needs a stable Internet connection to allow the drone to have high precision with RTK. Thus, in the paper the energy efficiency is not treated. In [21] an algorithmic work aiming for an Alpine application scenario is presented. The authors try to increase robustness and accuracy without compromising cost. Also in this case, the main goal is accuracy, and the energy efficiency and the latency are not evaluated. Another work that combines RTK-GNSS and mobile network is presented in [22]. The authors show how that the achieved high accuracy can be used in many application scenarios in the Internet of Things (IoT) paradigm.

LoRa is used in some previous work also as communication technology to achieve GPS-free localization [23], [24]. A combination of GNSS with LoRa is also presented in [7], where the authors use LoRa to cover the wide area of a harbor. However, in our approach, the LoRa technology is used additionally for RTK message broadcasting to several mobile devices to allow high-accuracy and energy efficiency. Very recently, commercial solutions, [25]–[28], are adding to other wireless communication standards, long range communication based on LoRa, summarized in TABLE I. Although these solutions exploit LoRa as an optional alternative to online correction data services to the best of our knowledge and from the information is possible to extract from their datasheets, none of the

available solutions provides an optimized solution to maximize both accuracy and energy efficiency.

III. Background

Satellite-based localization relies on a net of satellites in the medium earth orbits. Each of those satellites (SVs), broadcasts its local time together with its orbit. The mobile end-device on the ground (truck in Fig. 1) receives this data and stores it along with a receive timestamp. Subsequently, the end-device can calculate the satellite position from the transmitted time and orbit information.

To precisely determine the arrival timestamp, accurate local time is required. Without this information, there are four unknown variables: x, y, and z of the position and the time. Therefore the timestamp of the arrival and the position of four satellites are needed to evaluate the position of the mobile object [10]. As soon as the receiver's accurate time is found, three satellites are enough to calculate the distance to each SV and subsequent to trilateration the end-device position. Trilateration with three distances to three points results in two possible locations, where the solution in space can be discarded. Based on the available SVs and their position in the sky the end-device can estimate its position. However, this information is insufficient for an accurate calculation of its position that usually is in the range of 2-3 m.

There are multiple satellite systems from different organizations. Each of them works independently, but they can also be combined to have connections to enough satellites even when a part of the sky is obstructed. In addition, using more satellites can improve accuracy. Among other techniques, an effective way to further improve accuracy is using Differential GNSS [11]. The reference station calculates the distance using the arrival time of the signals received from the different satellites. It can calculate a correction factor simply by subtraction as it knows the real distance to the satellites. These will be valid for a radius of several hundred kilometers and can resolve the inaccuracies of orbits, satellite clocks, and effects of the ionosphere [10]. Modern GNSS modules are today also implementing another technique called Real Time Kinematics (RTK), which allows increasing the accuracy below 1 m (Fig. 1 on the right side).

A. Real Time Kinematics (RTK)

In RTK, instead of measuring just the time-of-arrival, the phase of the carrier is measured too. When the signal is emitted by the satellite it does travel a full number of complete cycles N plus the measured carrier phase until it is received at the user. This is shown in Fig. 2. The frequency of the carrier for GPS is 1575 MHz defining a wavelength of around 19 cm for the signals. But as long as the number of complete cycles N is not known, the distance is ambiguous. The resulting position with this ambiguity is called a Floating position in the language of RTK. If the N can be fixed to one number it is called a Fixed position. Finding the number of cycles with the inaccuracies of the GNSS would be impossible. Instead, the reference station idea from DGNSS is used. The reference station also called base station is measuring the carrier phase, too, as shown in Fig. 1. This measurement together with the accurate position of the base station is transmitted to the mobile unit also called rover. In RTK the module calculates the difference between the distances of the base and the rover

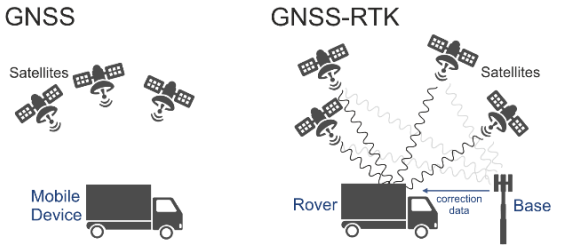

Fig. 1. The basic concept of standalone GNSS localization (left) and the principle of GNSS- RTK (right), where the base station measures the carrier phase and sends it to the rover, the mobile device.

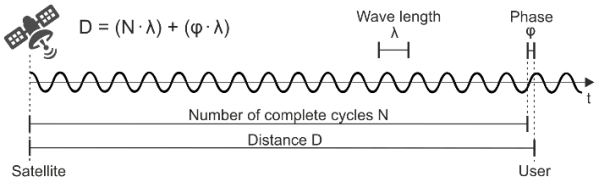

Fig. 2. Principle of measuring the phase in GNSS-RTK.

with the phase measurements, instead of calculating only the distance D to the satellite. The base station has to be in a radius up to 40 km to the rover to ensure that the signal is affected by the same inaccuracies as the rover. Therefore, it is easier to find the number of complete cycles N for the difference than for the distance to the satellite. When the difference is found, it can be used to calculate a relative vector from the base station to the rover. Finally, this is applied to the base station's absolute position to get a position with accuracy in the range of a few millimeters [10]. To exchange correction data between different vendors and providers, the standardized protocol Radio Technical Commission for Maritime Services (RTCM) is often used [11]. In this work, we exploit the low-power long-range capability of LoRa to transmit the RTCM information to achieve energy efficiency, low latency, and long-range and accurate positioning.

B. Low Power Long-Range Communication: LoRa.

LoRa is a proprietary spread spectrum modulation scheme from Semtech. It trades data rate for sensitivity and therefore increased range. It uses a chirp spread spectrum to increase robustness against channel degeneration such as multipath, fading, Doppler, and in-band jamming interferers [29]. A spreading factor, the bandwidth, and the frequency are defined depending on the bandwidth requirements, needed range, and network planning. The Spreading Factor (SF) ranges from SF5 to SF12, the bandwidth from 7.81 kHz to 500 kHz where SF5 500 kHz has the highest data rate and SF12 7.81 kHz has the lowest data rate but the highest range of 15-25 Km.

A LoRa packet is built out of a preamble, followed by a sync word and subsequent the payload. As LoRa itself only defines the physical layer, Semtech added the option to automatically add a header to the beginning of a packet with the payload length and a 16-bit checksum at the end. As the length is only encoded in 8 bits, the payload length in this mode is limited to 255 bytes. This mode is called an explicit header. LoRa defines the protocol only on the physical layer, which allows the building of an own protocol on top of that. In addition, LoRa enables not only point to point communication but also offers the possibility for multicast.

IV. RTK-LoRa Proposed Approach

Our proposed approach, called RTK-LoRa, utilizes LoRa as a wireless communication interface between the base station and the moving rover, as shown in Fig. 3. This data link to an always-active local GNSS receiver allows not only the transfer of RTCM correction data but also to request current orbits from the base station, thus eliminates the need to download orbits from the satellites when the GNSS signals are weak.

A. RTK and LoRa Communication

For communicating with the base station, LoRa is used in the explicit header mode, as described in Section III, with the spreading factor SF7 and a bandwidth of 250 kHz. In the explicit header mode, only the payload has to be sent to the LoRa IC and a header containing the payload length and a checksum is added automatically. At the receiver, the checksum is controlled by the module and an interrupt is generated. The explicit header mode is limited to a payload length of 255 bytes [30], which is typically lower than the RTCM correction data and the orbit information. To have the ability to send longer messages and to differentiate between message types an Enumeration Segmentation Reconstruction (ESR) algorithm is implemented.

The structure of one segment, which is a part of one message, is shown in Fig. 4. Each segment contains a header with three fields. The first field is a message-id increased after every sent message. This allows the detection of a new message even when the last message was not finished. The second field contains the message type summarized in TABLE II. The last field holds the number of remaining segments which is zero when the last segment of the message is received.

B. An Energy-Efficient Algorithmic Approach.

An efficient way to reduce the energy consumption of an embedded device is Duty Cycling (DC), i.e., switching-off subsystems when they are not needed. Although longer off-periods are simply applicable if latency is not of concern, its application on GNSS receivers is typically fraught with problems. To determine the receiver's position, the exact local time, as well as the current orbits of the satellites, are required. If this information is not present, as it is the case after disabling the receiver, time-consuming and error-prone downloading is needed. Therefore, the available information after the start is essential to reduce the time-to-first-fix (TTFF), and thus the energy consumption in duty cycled operation. Methods aiming to reduce the time-to-first-fix by providing additional information such as almanac and ephemeris data, time, Doppler frequencies, or previous positions are commonly referenced to as Assisted GNSS [29].

TABLE II. Available message types used for ESR

Type ID	Name	Purpose
1	RTCM	Correction data for GNSS
2	DB Request	Request to send to current orbits
3	DB Response	Current orbits
4	RTK Control	Instruct the base station to start/stop sending correction data

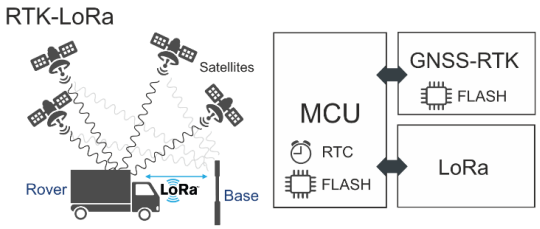

Fig. 3. Principle of RTK-LoRa, where the base station measures the carrier phase and sends it to the rover via LoRa. Orbit information can be requested from the always-on base station via the data connection or stored locally on the energy-optimized mobile device.

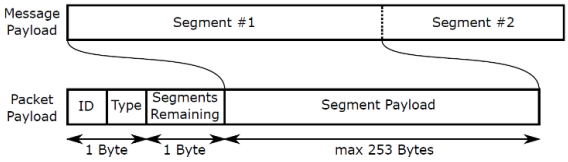

Fig. 4. Structure of an ESR packet.

One of this paper's goals and contributions is to provide an energy-efficient model to reduce energy consumption without losing performance in terms of latency and precision.

MCU Assisted GNSS – In this work, the benefits of Assisted GNSS on the receiver energy consumption is analyzed and exploited. In particular, the real-time clock (RTC) of a microcontroller (MCU) is used to preserve the time information during the GNSS module's deactivation. Furthermore, orbit data and the last position is provided after cold start. In the proposed approach, this is done in three different ways. For GNSS modules hosting an accessible flash memory, the data can be stored directly on the module without additional memory requirements. Alternatively, the data can be stored in the MCU's memory and updated directly after the activation of the GNSS module. Finally, with the available LoRa module and the RTK-LoRa implementation, valid orbit data can be requested directly from the always-on base station, which streams the RTCM information periodically. A simplified version of the proposed MCU assisted LoRa-RTK for a GNSS module with flash storage for the navigation database is as following:

Algorithm 1 LoRa-RTK

```
1:  Function RTK-LoRa with internal flash memory
2:    MCU wake-up event                                   START
3:    if orbits not outdated
4:      activate GNSS module
5:      update navigation database from module flash
6:      update local time from MCU
7:    else
8:      request current orbits from base station
9:      activate GNSS module
10:     update current orbits
11:     update local time from MCU
12:   end if
13:   while active GNSS do
14:     while RTCM message not reconstructed do           SENSING
15:       receive ESM packages
16:     end while
17:     update RTCM data
18:   end while
19:   update RTC from GNSS module                         STOP
20:   deactivate GNSS section
21:   backup navigation data in module flash
22:   hibernate sensor node
```

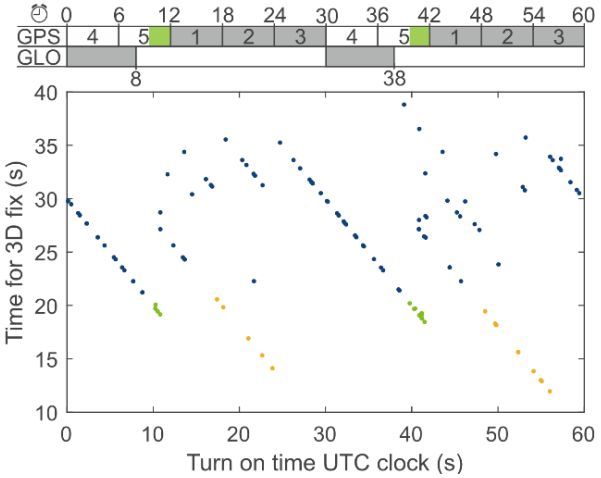

Fig. 5. Influence of the orbit broadcast schedule on the time-to-first-fix.

One-Shot Localization – A second proposed approach of this work, aiming to reduce time-to-first-fix without the requirement of locally available orbit data or an additional data link in duty cycled operation is the synchronization to orbit broadcast schedules. An experimental evaluation of the turn-on time and its influence on the time-to-first-fix is shown in Fig. 5. The GNSS module was randomly activated, and the turn-on time together with the duration until the first 3D fix was logged. The upper part of the figure shows the GPS and GLONASS schedules with gray marked orbit transmission windows. It can be seen that the activation of the module just before a broadcast can reduce the time-to-first fix to 18 s for GPS, marked in green. Although GLONASS would allow reducing this time even further, the limited number of satellites makes a robust localization unlikely. The implementation on the sensor node uses the RTC of the microcontroller to synchronize with the orbit schedule.

This paper exploits and combines the two approaches to achieve both energy efficiency and low latency of localization, compared to the baseline duty cycling approach, reducing the time to first RTK fix by up to 20 s. A sensor node will be designed to analyze the proposed approach's benefits with accurate measurements in the following section.

TABLE III. PERFORMANCE SUMMARY OF 3 GNSS MODULES USED IN THIS EVALUATION

	ZOE-M8B	**NEO-M8P**	**ZED-F9P**
Vendor	u-blox	u-blox	u-blox
Supported global receiver types	GPS, BeiDou, GLONASS, Galileo	GPS, BeiDou, GLONASS	GPS, BeiDou, GLONASS, Galileo
Release	2016	2016	2019
Antenna	Passive	Active	Active
RTK	No	Yes	Yes
Update rate	-	8 Hz	20 Hz
Accuracy	2.5 m	0.025 m	0.01 m
Size	4.5 × 4.5 × 1.0 mm	12.2 × 16 × 2.4 mm	17 × 22 × 2.4 mm
Typ. supply voltage	1.8 V	3 V	3 V
Typ. power consumption [a]	58.5 mW	75 mW	204 mW

[a.] typical power consumption during tracking in GPS only mode

V. SYSTEM ARCHITECTURE AND IMPLEMENTATION

Fig. 6 (a) shows a simplified block diagram of the proposed high-precision wireless sensor node to evaluate RTK-LoRa. Fig. 6 (b) shows the designed and implemented sensor node that can host GNSS modules and radio modules through three plug-and-play ad-hoc sockets. The sockets are perfect for evaluating different subsystems and are occupied by the ZED-F9P module from u-blox and the most recent LoRa SX-1261 IC from Semtech in the lower part of the figure. Processing is performed on an STM32L452 microcontroller from STMicroelectronics, which is based on an ARM Cortex-M4F running at up to 80 MHz. The microcontroller is optimized for low-power operation and consumes typical 36 µA per MHz. The sensor node includes a power management subsystem that is able to host a 3.7 V Li-Ion rechargeable battery, and it provides efficient 3.3 V and 1.8 V for the whole system. As the sensor board has been designed with energy efficiency in mind, the novel Semtech SX1261 LoRa integrated circuit has been used, featuring an up to 50 % lower current consumption during receive mode and about 10 % current savings during transmit mode, while enabling higher output power compared to the popular predecessor SX1276. Moreover, the SX1261 can operate with a lower supply voltage (1.8 V instead of 2.3 V), which results in additional power savings.

In this work, we evaluated three different GNSS modules to have the best fit in terms of accuracy and power consumption, listed in TABLE III. The three different GNSS receivers have been chosen with power consumption in the range of tens to hundreds of mW. The u-blox ZOE-M8B module, with its Super-E mode, is optimized for low-power applications and it is shipped in a space-saving System in Package (SiP) [31]. This receiver does not support RTK but is selected as a reference point for low-power GNSS positioning. Moreover, its localization performance can give a baseline to appreciate the benefits of RTK to achieve high accurate geo-localization. The other two receivers support RTK, in particular, we evaluated the u-blox NEO-M8P module [32] and u-blox ZED-F9P which was released in March 2019 [33].

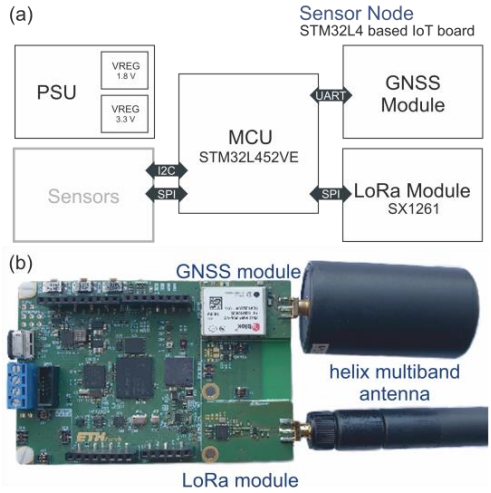

Fig. 6. (a) High-level block diagram of the designed board that includes a Cortex M4 microcontroller and the two LoRa and RTK modules and can be used either as a base station or rover. (b) The prototype of the sensor node developed to perform in-field tests of the proposed solution.

VI. Experimental Results

The developed prototype shown in Fig. 6 (b) has been employed to carry out all the performance evaluations in terms of power consumption, functionality, and localization accuracy. Conventional GNSS measurements were taken on the geographical reference point CH030000109110913000 (N47.407907091 °, E8.497057370 °, A575.631 m) as ground-truth. Static GNSS-RTK measurements were conducted on a building's roof-top under perfect conditions of clear sky with 1 m distance between the base station and the rover. The base station position has been determined with a one-hour calibration measurement controlled by the u-center GNSS evaluation software. During the evaluation, the determined base station position has been configured with a measurement confidence of 1 mm. Thus, inaccuracies due to a wrong base station position will result in an offset but will not further influence the differential approach of GNSS-RTK. As ground-truth, the rover position was determined from the distance and angle to the base station.

Subsection VI.A shows an evaluation of different tested GNSS antennas. In subsection IV.B the correlation between on time and accuracy is analyzed for conventional GNSS operation. Subsection IV.C shows the performance and the influence of the proposed RTK-LoRa and its optimizations during GNSS-RTK positioning, followed by an in-field evaluation in an urban scenario in subsection D. Finally, subsection E concludes the experimental results with a comparison of the trade-off between energy consumption and positioning accuracy in duty cycled operation.

A. Antenna evaluation

Prior the characterization of the GNSS modules, four different antennas, listed in TABLE IV. , have been tested in terms of carrier-to-noise-ratio (CNR), power consumption, and reported accuracy. For the measurement, the different antennas are connected side by side to multiple ZED-F9P modules, respectively to the ZOE-M8B module for the passive antenna. The compact 25 mm x 25 mm sized patch antenna MIA1516 shows the lowest CNR for all satellite elevation angels with an average of -5 dB(Hz) compared to the antenna with the highest CNR. For elevation angels higher than 20° the multiband patch antenna shows the best CNR, outperforming the helix antennas by 2 dB(Hz).

In addition to the CNR, the energy consumption of the active antenna has to be considered during the design phase. On the example of the ZED-F9P the module consumption during acquisition increases by 10 %, or more specifically, by 32 mW when the helix multiband antenna is used and not the ANN-MB-00 antenna from u-blox. The deactivation of the analog receiver part allows determining the energy consumption of the active antenna as 31 mW, 53.5 mW, and 85.5 mW for MIA1516, ANN-MB-00, and M1227HCT, respectively. The influence of the antenna selection on the static GNSS-RTK accuracy is shown in Fig. 7. The data was acquired after the rover reported an RTK fix. Both multiband antennas allow a comparable accuracy of ±1 cm. It can be concluded that both multiband antennas allow reaching the maximal accuracy, with comparable CNR but in the case of the u-blox antenna at lower energy consumption. If it can be tolerated to reduce accuracy for higher energy efficiency, a single band antenna or even a passive antenna can be used.

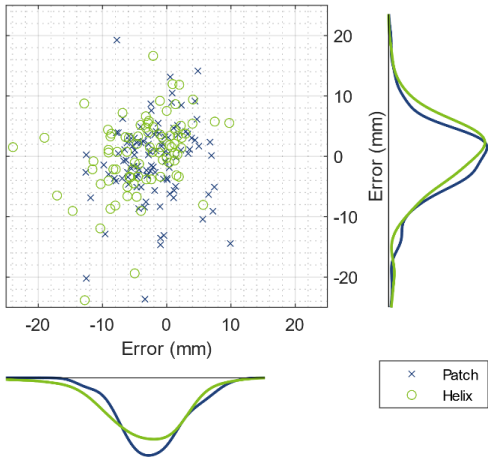

Fig. 7. Static reported GNSS-RTK accuracy ZED-F9P with ANN-MB-00 patch antenna and M1227HCT helix antenna.

TABLE IV. Evaluated Antennas

Vendor	Product	Type	Power	Multiband
MAXTENA	M1516HCT	Helix	Passive	-
MAXTENA	MIA1516	Patch	Active	
MAXTENA	M1227HCT	Helix	Active	Yes
u-blox	ANN-MB-00	Patch	Active	Yes

B. GNSS evaluation in static conditions

The energy consumption of GNSS in deep-duty cycled operation is typically dominated by the start-up time of the used module. For that reason, the relationship between positioning accuracy and active time has been analyzed, as shown in Fig. 8. To compare the three modules the RTK functionality has been disabled, and the reported accuracy was logged for 30 seconds in the initial condition of "cold", "warm", "hot" and "MCU"-start. During the cold start, no time and satellite information are available on the module. In contrast to that, valid time, almanacs, and ephemerides data are stored in the module's memory for hot-start, respectively, time and almanacs data for warm start. The low-power optimized module ZOE-M8B allows, with the AssistNow Autonomous feature, a more advanced warm start. It calculates the satellite position from old ephemerides information and reduces the warm start time significantly compared to the other modules. In addition to the configurations available directly on the GNSS modules, the microcontroller-assisted start described in section IV.B is analyzed.

To allow statistical analysis, measurements have been repeated 20 times for each configuration, and the average is shown in the top row Fig. 8. The lower row shows the time until the module reports the accuracy milestones of 3D fix, 3 m circular error probable (CEP), and 2 m CEP. The error bar illustrates when 10 % and 90 % of the measurements pass the targeted accuracy. It can be seen, that all three modules need typical 20 s to achieve an accuracy below 2 m after a cold-start. Warm-start does not significantly reduce the time-to-first-fix but increases the accuracy of the NEO-M8P module. If warm-start is combined with the AssistNow

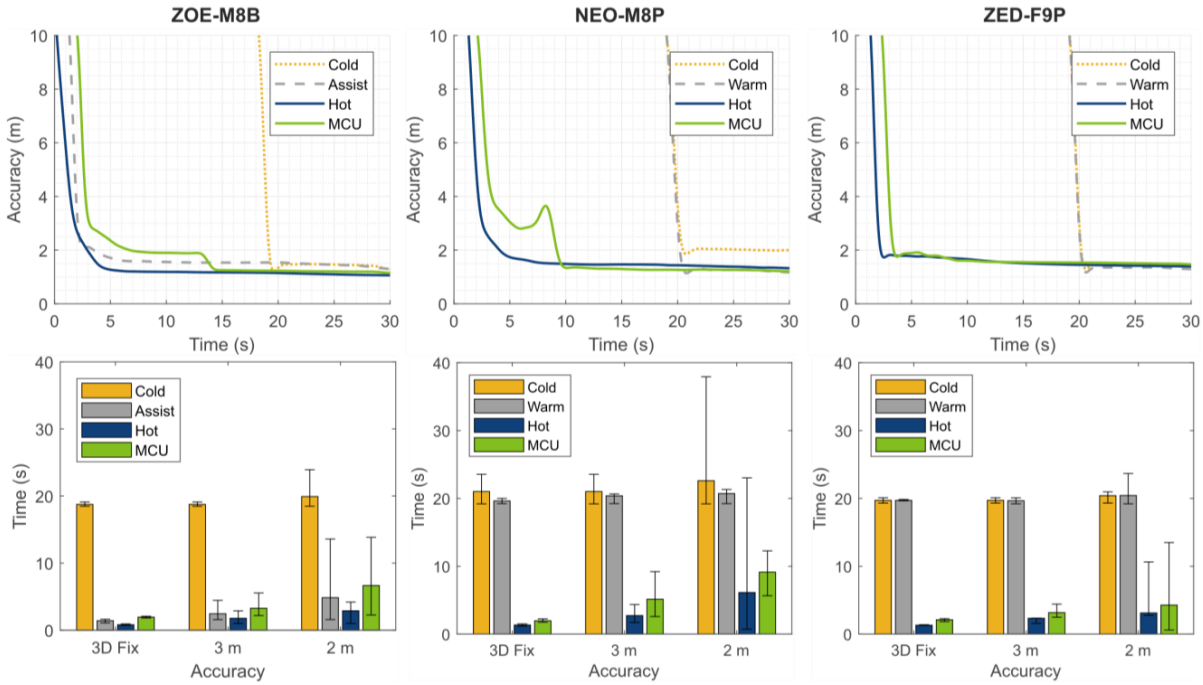

Fig. 8. Experimental evaluation of the GNSS accuracy over time from different initial conditions.

Autonomous feature the ZOE-M8B module needs typically 3.5 s to reach 2 m accuracy. The latest and most power-hungry module ZED-F9P reaches 2 m accuracy after 1.32 s during hot-start in optimal conditions.

Although our proposed MCU-based assisted GNSS does not allow to outperform the AssistNow Autonomous feature of the ZOE-M8B in terms of time-to-first-fix, it allows to reach the maximal achievable accuracy faster. In contrast to that, for GNSS modules without AssistNow Autonomous, the implemented assisted GNSS brings a tremendous reduction for the time-to-first-fix, and the maximal accuracy is reached faster. A summary of the improvements for duty-cycled operation is given in TABLE V.

C. GNSS RTK evaluation

An analysis of the time-to-first-fix during RTK positioning, together with the precision degeneration introduced by the base station's distance when transmitting the correction data via LoRa is shown in Fig. 9. The timing is analyzed as an average out of multiple measurements for the three operational states of, a conventional GNSS positioning with a precision of 2.5 m circular error probable, RTK float, and RTK fixed. To determine the benefits of additional satellite information after cold start, the last valid orbit positions were either stored locally in the GNSS modules' flash memory or on the microcontroller. Additionally, the LoRa connection was used to share the base station orbits with the module after cold-start. The NEO-M8P module needs on average additional 100 s after cold start until an RTK fix is established. For all initial conditions, the time until an RTK fix is achieved shows high variation but is typically below 140 s. In contrast to that, the ZED-F9P requires only 13 additional seconds after the cold start or in total 33 s to reach an RTK fix. The NEO-M8P module profits most from recent orbit information provided via the base station. If the last orbit data is stored locally in the ZED-F9P module flash, the time-to-first-RTK-fix can be reduced from 33 s to 13 s comparable to the hot-start performance.

The influence of the distance between base station and rover on the reported accuracy is shown right in Fig. 9. The measurements have been conducted in a rural area. For both devices, ZED-F9P modules with LoRa for the correction data exchange have been used. The precision is reduced from 5.7 mm CEP at 1 km distance to 9.3 mm CEP at 3 km.

D. Urban Canyon

Fig. 11 shows an in-field test performed in the urban area of Zurich in Switzerland, with a base station and a mobile rover. For this experiment, the u-blox ZED-F9P modules with the ANN-MB-00 antennas were used. The base station has been placed on the roof-top of a building with a clear view across the city (white marker) while the rover was moving through the city. During the measurement, the rover was configured to log the route together with the reported accuracy and the received RTCM correction data packages. Fig. 11 (b) shows the position and frequency of received data packages from the base station. It can be seen that the city center and the area overseen by the base station show a high data reception rate. In contrast to that, parts of the obstructed route show sparse or no reception of correction data. The verification of the reported position accuracy during the route is shown in Fig. 11 (c). The measurement shows that the reported accuracy decreased twice above 1 m, visualized in yellow. In both cases, the sky was obstructed by buildings, respectively, an underpass. Typically, the reported average accuracy was 20 cm with peaks of below 10 cm. The lower part of Fig. 11 shows three characteristic enlargements during the route through the city. The subfigure (d) shows an enlargement at Zurich Quaibrücke with 1.3 km distance to the base station. The perfect conditions of open view and close distance result in a high package rate, marked as white points, and a reported accuracy below 10 cm. The markings on the

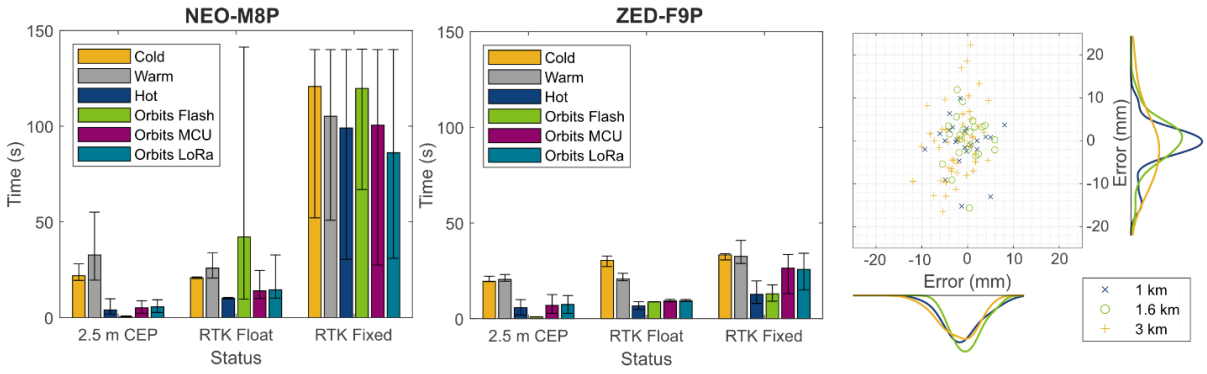

Fig. 9. Experimental evaluation of the GNSS-RTK accuracy over time from different initial conditions and warm-start data storage policies. Influence of the distance between the base station and the rover on the precision in static conditions.

bridge also allow verifying the reported position with the actual position. Subfigure (e) shows the logged position during the lost connection in the underpass of train station Tiefenbrunnen, at 3.1 km distance to the base station. The increased localization performance of GNSS-RTK despite sparse correction data exchange is shown in subfigure (f). The reported accuracy stays below 20 cm, also minutes after the last update of the correction information.

E. Energy consumption

A summary of the energy consumption to reach a targeted accuracy in duty-cycled operation is shown in Fig. 10. The low power optimized ZOE-M8B allows determining a rough position of approximately 100 m with an average energy consumption below 1 J. To reach the GNSS accuracy limit of 2 m CEP, 2.3 J are required. In the case of an active AssistNow Autonomous feature, the same accuracy can be achieved with less than 1 J. If the application requires the accuracy of GNSS-RTK, the faster time-to-first-fix of the ZED-F9P allows compensating for the higher power consumption with an average of 12 J from cold-start and 5.6 J with the assisted algorithm.

A summary of the average time to reach a reported accuracy of 2 m CEP and to obtain the a RTK fix together with the energy consumption is given in TABLE V. In fact, the proposed assisted GNSS approach allows to reduce the energy consumption in duty-cycled operation by 76 % (GNSS) and 53 % (GNSS-RTK) for the ZED-F9P module and by 67 % (GNSS) and 21 % (GNSS-RTK) for the NEO-M8P module.

During duty-cycled operation, 90 % of the energy consumption is caused by the ZED-F9P GNSS module and only 3 % by the LoRa transceiver.

TABLE V. SUMMARY AVERAGE LOCALIZATION TIME AND ASSOCIATED ENERGY CONSUMPTION

		ZOE-M8B	NEO-M8P	ZED-F9P
2 m CEP	cold	20 s / 2.3 J	23 s / 3.4 J	20 s / 6.2 J
	assisted GNSS[b]	5 s / 0.9 J	9 s / 1.1 J	4 s / 1.8 J
RTK fix	cold	-	121 s / 14 J	33 s / 12 J
	assisted GNSS	-	86 s / 11 J	13 s / 6 J

[b] AssistNow Autonomous for ZOE-M8B, proposed algorithm for NEO-M8P and ZED-F9P.

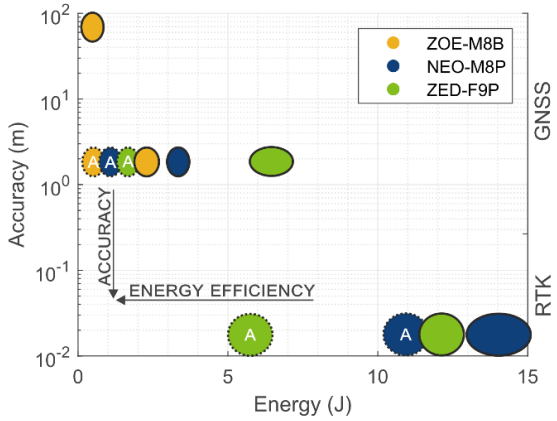

Fig. 10. Comparison of the energy consumption from cold-start for different target accuracy configurations. The deviation is indicated by the shape and the assisted GNSS optimized results are marked as "A".

VII. CONCLUSION

This paper presented the design and the implementation of a novel sensor node that combines low power and long-range communication with Real-Time Kinematic GNSS to achieve both high accuracy and energy efficiency. The sensor nodes modularity has been exploited to evaluated and compare state-of-the-art GNSS modules in terms of localization accuracy, time-to-first-fix, and energy efficiency. The implemented energy optimizations based on assisted GNSS allowed to reduce the time-to-first-fix by 20 s and thus the GNSS-RTK energy consumption by 53 % during duty cycled operation. Experimental evaluation, including measurements in the urban area of Zurich, has shown the benefits of the combination RTK-LoRa in terms of precision even at kilometers of distance. Without using costly infrastructures, the proposed solution achieved an overall precision of 20 cm in an urban area test-bed with peak values of below 10 cm.

The results suggest that the GNSS-RTK implementation exploiting LoRa maintains high reported accuracy despite a low correction data exchange rate. Thus the correlation of correction data rate and accuracy degeneration can be an interesting next research question to further optimize energy consumption without compromising reliability.

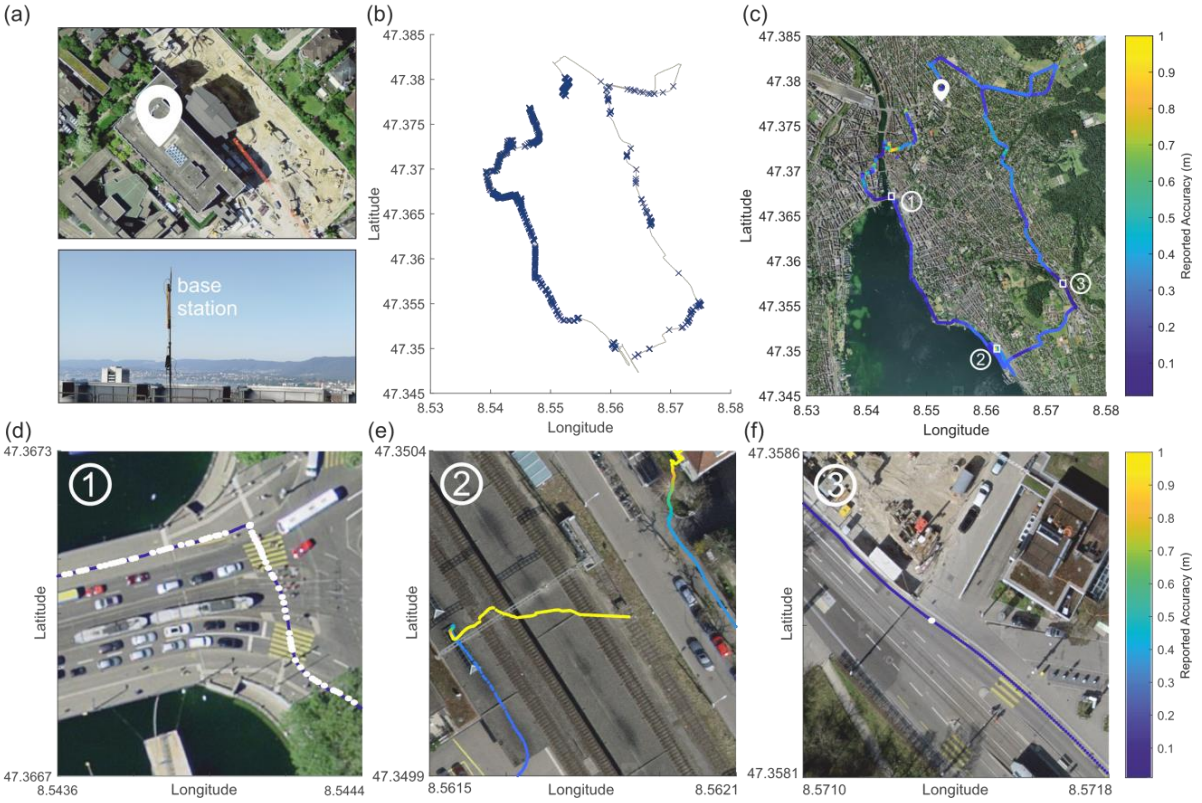

Fig. 11. In-field test in the urban area of Zurich. (a) Base station placed on the roof-top of a building with clear view over the city center. (b) Route through the city with marked reception of RTCM correction data packages. (c) Reported rover accuracy while moving through the city by bike. The markings show the position of the base station and the enlargements. (d) Maximal accuracy at Zurich Quaibrücke, the received RTCM data packages are marked as white points. (e) Connection loss in underpass of train station Tiefenbrunnen. (f) High reported accuracy despite sparse reception of RTCM correction data in Zurich Hottingen.

ACKNOWLEDGMENT

This work was in part funded by the WSL Institute for Snow and Avalanche Research (SLF).

REFERENCES

[1] Blewitt Geoffrey, *Basics of the GPS Technique: Observation Equations*. Swedish Land Survey, 1997.

[2] O. Heirich, P. Robertson, A. C. García, T. Strang, and A. Lehner, "Probabilistic localization method for trains," in *IEEE Intelligent Vehicles Symposium, Proceedings*, 2012, pp. 482–487, doi: 10.1109/IVS.2012.6232194.

[3] H. R. Hosseinpoor, F. Samadzadegan, and F. Dadras Javan, "Precise Target Geolocation Based on Integration of Thermal Video Imagery and RTK GPS in UAVS," *ISPRS - Int. Arch. Photogramm. Remote Sens. Spat. Inf. Sci.*, vol. XL-1-W5, no. 1W5, pp. 333–338, Dec. 2015, doi: 10.5194/isprsarchives-XL-1-W5-333-2015.

[4] M. Loriot, A. Aljer, and I. Shahrour, "Analysis of the use of LoRaWan technology in a large-scale smart city demonstrator," in *2017 Sensors Networks Smart and Emerging Technologies, SENSET 2017*, Nov. 2017, vol. 2017-Janua, pp. 1–4, doi: 10.1109/SENSET.2017.8125011.

[5] P. Mayer, M. Magno, T. Brunner, and L. Benini, "LoRa vs. LoRa: In-Field Evaluation and Comparison for Long-Lifetime Sensor Nodes," in *Proceedings - 2019 8th International Workshop on Advances in Sensors and Interfaces, IWASI 2019*, Jun. 2019, pp. 307–311, doi: 10.1109/IWASI.2019.8791362.

[6] M. Magno, F. A. Aoudia, M. Gautier, O. Berder, and L. Benini, "WULoRa: An energy efficient IoT end-node for energy harvesting and heterogeneous communication," in *Proceedings of the 2017 Design, Automation and Test in Europe, DATE 2017*, May 2017, pp. 1528–1533, doi: 10.23919/DATE.2017.7927233.

[7] I. F. Priyanta, F. Golatowski, T. Schulz, and Di. Timmermann, "Evaluation of LoRa Technology for Vehicle and Asset Tracking in Smart Harbors," in *IECON Proceedings (Industrial Electronics Conference)*, 2019, pp. 4221–4228.

[8] B. Bellini, J. P. Becoña, A. S. Pereira, C. Vázquez, and A. Arnaud, "IoT in the agribusiness, a power consumption view," in *Proceedings - IEEE International Symposium on Circuits and Systems*, 2019, vol. 2019-May, doi: 10.1109/ISCAS.2019.8702576.

[9] L. Farhan, O. Kaiwartya, L. Alzubaidi, W. Gheth, E. Dimla, and R. Kharel, "Toward Interference Aware IoT Framework: Energy and Geo-Location-Based-Modeling," *IEEE Access*, vol. 7, pp. 56617–56630, 2019, doi: 10.1109/ACCESS.2019.2913899.

[10] P. Bissig, M. Eichelberger, and R. Wattenhofer, "Fast and Robust GPS Fix Using One Millisecond of Data," in *2017 16th ACM/IEEE International Conference on Information Processing in Sensor Networks (IPSN)*, 2017, pp. 223–234.

[11] M. Magno, S. Rickli, J. Quack, O. Brunecker, and L. Benini, "Poster Abstract: Combining LoRa and RTK to Achieve a High Precision Self-Sustaining Geo-Localization System," in *Proceedings - 17th ACM/IEEE International Conference on Information Processing in Sensor Networks, IPSN 2018*, Oct. 2018, pp. 160–161, doi: 10.1109/IPSN.2018.00043.

[12] P. Mayer, M. Magno, A. Berger, and L. Benini, "RTK-LoRa: High-Precision, Long-Range and Energy-Efficient Localization for Mobile IoT devices," in *2020 IEEE Sensors Applications Symposium (SAS)*, Mar. 2020, pp. 1–5, doi: 10.1109/SAS48726.2020.9220057.

[13] N. Zhu, J. Marais, D. Betaille, and M. Berbineau, "GNSS Position Integrity in Urban Environments: A Review of Literature," *IEEE Trans. Intell. Transp. Syst.*, vol. 19, no. 9, pp. 2762–2778, Sep. 2018, doi: 10.1109/TITS.2017.2766768.

[14] A. Stern and A. Kos, "Positioning performance assessment of geodetic, automotive, and smartphone gnss receivers in standardized road scenarios," *IEEE Access*, vol. 6, pp. 41410–41428, Jul. 2018, doi: 10.1109/ACCESS.2018.2856521.

[15] J. Lesouple, T. Robert, M. Sahmoudi, J. Y. Tourneret, and W. Vigneau, "Multipath Mitigation for GNSS Positioning in an Urban Environment Using Sparse Estimation," *IEEE Trans. Intell. Transp. Syst.*, vol. 20,

no. 4, pp. 1316–1328, Apr. 2019, doi: 10.1109/TITS.2018.2848461.

[16] F. Zhu, Z. Hu, W. Liu, and X. Zhang, "Dual-Antenna GNSS Integrated with MEMS for Reliable and Continuous Attitude Determination in Challenged Environments," *IEEE Sens. J.*, vol. 19, no. 9, pp. 3449–3461, May 2019, doi: 10.1109/JSEN.2019.2891783.

[17] P. Sommer *et al.*, "Energy- And Mobility-Aware Scheduling for Perpetual Trajectory Tracking," *IEEE Trans. Mob. Comput.*, vol. 19, no. 3, pp. 566–580, Mar. 2020, doi: 10.1109/TMC.2019.2895336.

[18] J. Liu *et al.*, "CO-GPS: Energy efficient GPS sensing with cloud offloading," *IEEE Trans. Mob. Comput.*, vol. 15, no. 6, pp. 1348–1361, Jun. 2016, doi: 10.1109/TMC.2015.2446461.

[19] D. Gebre-Egziabher, "Evaluation of Low-Cost, Centimeter-Level Accuracy OEM GNSS Receivers," 2018. [Online]. Available: http://www.dot.state.mn.us/research/reports/2018/201810.pdf.

[20] I. Um, S. Park, H. T. Kim, and H. Kim, "Configuring RTK-GPS Architecture for System Redundancy in Multi-Drone Operations," *IEEE Access*, vol. 8, pp. 76228–76242, 2020, doi: 10.1109/ACCESS.2020.2989276.

[21] P. Henkel and B. Banjara, "Precise Positioning in Alpine Areas with Troposphere and Multipath Estimation," *IEEE Sens. J.*, vol. 18, no. 20, pp. 8397–8409, Oct. 2018, doi: 10.1109/JSEN.2018.2865769.

[22] B. Rokaha, B. P. Gautam, and T. Kitani, "Building a Reliable and Cost-Effective RTK-GNSS Infrastructure for Precise Positioning of IoT Applications," in *2019 Twelfth International Conference on Mobile Computing and Ubiquitous Network (ICMU)*, Nov. 2019, pp. 1–4, doi: 10.23919/ICMU48249.2019.9006632.

[23] A. Mackey and P. Spachos, "LoRa-based Localization System for Emergency Services in GPS-less Environments," in *INFOCOM 2019 - IEEE Conference on Computer Communications Workshops, INFOCOM WKSHPS 2019*, Apr. 2019, pp. 939–944, doi: 10.1109/INFCOMW.2019.8845189.

[24] I. Amadou, B. Foubert, and N. Mitton, "LoRa in a haystack: A study of the LORA signal behavior," in *International Conference on Wireless and Mobile Computing, Networking and Communications*, Oct. 2019, vol. 2019-October, doi: 10.1109/WiMOB.2019.8923319.

[25] Emld Ltd., "REACH RS2," 2019. http://files.emlid.com/docs/Datasheet RS2 ENG web.pdf (accessed Jul. 08, 2020).

[26] eFarmer B.V., "FieldBee L2 receiver," 2019. https://www.fieldbee.com/wp-content/uploads/2019/12/FieldBee-RTK-L2-receiver.pdf (accessed Jul. 08, 2020).

[27] LOCOSYS Technology Inc., "RTK-M100," 2019. https://www.locosystech.com/Templates/att/RTK-M100_EDM_v1.0.pdf?lng=en (accessed Jul. 08, 2020).

[28] marXact B.V., "marxact UNI-GR1," 2020. https://marxact.com/specsunigr1.pdf (accessed Jul. 08, 2020).

[29] Z. Jean-Marie, *GPS Essentials of Satellite Navigation*. u-blox AG, 2009.

[30] Semtech, "SX1261/2 Long Range, Low Power, sub-GHz RF Transceiver," 2019. https://semtech.my.salesforce.com/sfc/p/#E0000000JelG/a/2R000000HT7B/4cQ1B3JG0iKRo9DGRkjVuxclfwB.3tfSUcGr.S_dPd4 (accessed Jun. 30, 2020).

[31] u-blox AG, "ZOE-M8B SiP," 2018. https://www.u-blox.com/sites/default/files/ZOE-M8B_ProductSummary_%28UBX-17012173%29.pdf (accessed Jun. 30, 2020).

[32] u-blox AG, "NEO-M8P," 2020. https://www.u-blox.com/sites/default/files/NEO-M8P_ProductSummary_%28UBX-15015836%29.pdf (accessed Jun. 30, 2020).

[33] u-blox AG, "ZED-F9P," 2020. https://www.u-blox.com/sites/default/files/ZED-F9P_ProductSummary_(UBX-17005151).pdf (accessed Jun. 30, 2020).